Further Investigations of Disk Dynamics with an Embedded Protoplanet

Chris Orban

November 3, 2004

Abstract

Extrasolar planet searches have found a statistically significant number of systems with gas-giant planets orbiting at distances closer than that of Mercury in our own solar system. Our current understanding suggests that these planets do not form there, instead a protoplanetary core will migrate to those positions through interactions with the the protoplanetary disk. This study is an extension of 2-D hydrodynamic simulations of this phenomena presented in Josef Koller's PhD. thesis, "Potential Vorticity Evolution in the Co-orbital Region of Embedded Protoplanets," with the motivation to resolve convergence issues in the plot of the azimuthally averaged potential vorticity of the disk which strongly affect the torque evolution of the protoplanet. Higher resolution simulations using more robust codes have shown that the vortex production does not occur in the same location that the previous simulations suggest, and that the lack of convergence was due to unresolved structure in the co-orbital region. There are still other numerical concerns, but an important feature of the azimuthally averaged potential vorticity is now understood.

1 Introduction

As of July 2004, 123 planets outside of our solar system have been discovered (The Extrasolar Planets Encyclopedia 2004). This has sparked considerable interest in the public and astronomers alike of the nature of these newly discovered worlds, and the possibility of better understanding the origins of our solar system as well as the allure of discovering earth-like planets and perhaps eventually detecting life.

The technique responsible for the success of extrasolar planet searches is the Doppler shift method. The tug of the planet in orbit around the star causes minute changes in the wavelength of the star's spectral lines which are detectable from earth. Although the Doppler shift method is particularly sensitive to finding large planets in close orbits to the parent stars, there appears to be a statistically significant number of systems with gas-giant planets orbiting at distances closer in than the orbit of Mercury to the sun. (Udry et al. 2003)

Our current understanding suggests that gas-giant planets form from gravitational accretion onto a small rocky core about ten times the mass of the earth. This protoplanetary core is embedded in a disk of gas and dust, at distances comparable to the orbits of Jupiter and Saturn. Thus the problem of explaining the surplus of gas-giants in close orbits involves explaining the migration of the protoplanetary core from those distances to the scorchingly hot orbits where planets have been found.

There has been a number of studies, both analytic and numerical to investigate the gravitational torque on the protoplanetary core in the disk and infer the timescale of migration. Gravitational scattering has been considered. This can can occur when an asteroid is deflected to the outer solar system by Jupiter, for example. As a result, Jupiter inches closer to the sun from conservation of momentum. It is thought that this effect, or interactions with other planets is not strong enough to explain tight orbits

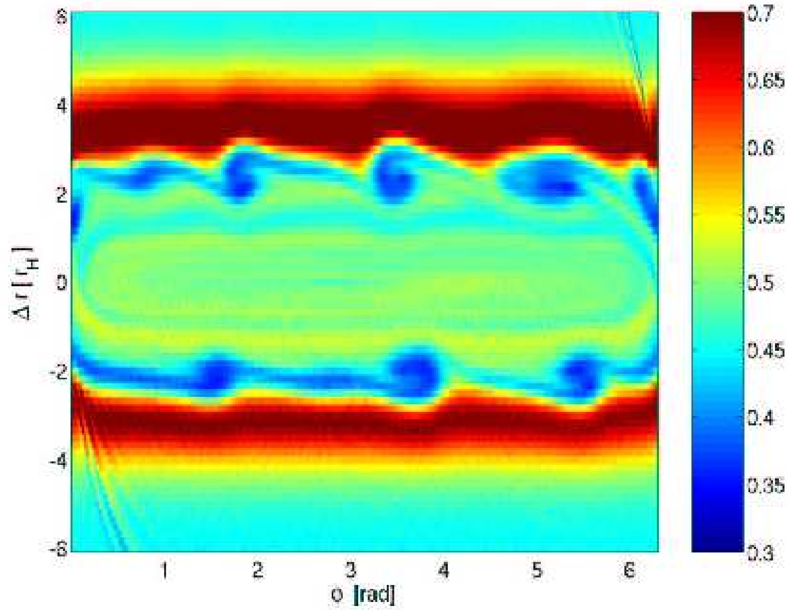

Figure 1: A snapshot of a protoplanetary disk simulation from Josef Koller's Ph.D. Thesis. Color indicates potential vorticity, $(\nabla \times \mathbf{v})/\Sigma$ where $\mathbf{v}$ is the velocity vector and Σ is the surface density. The planet is located at $\Delta r = 0$, $\phi = 0$. Vortices can be seen that make close encounters with the planet causing rapid oscillations in torque. (Figure courtesy of Josef Koller)

of extrasolar planets. The interactions with the disk are likely the primary cause of migration. (Koller 2004 and references therein)

From modeling of infrared, radio and optical observations, the disk is semi-empirically estimated to have a lifetime between $10^6 - 10^7$ years (Hollenback et al. 2000) which places another constraint on migration scenarios. Josef Koller's 2004 Ph.D. thesis, "Potential Vorticity Evolution in the Co-orbital Region of Embedded Protoplanets," provides a good review of the literature on protoplanetary migration. The results presented here are an extension of that numerical work at higher resolutions motivated by some very important convergence-related issues which strongly affect the torque on the planet. (Josef Koller will often be abbreviated JK in this report.)

Josef conducted "brute force" 2-D hydrodynamic simulations of a protoplanetary core embedded in a disk to investigate the role of vortices on the torque evolution and studied a quantity called potential vorticity to better understand the disk dynamics. Among his results was the conclusion that the torque evolution consisted of three phases. In phase I, the planet core experienced negative torques modulated by a period similar to the libration period. ($\tau_{lib} = \sqrt{4/27\mu} \sim 40P$ where P is the period of the planet. This is the same period as particles orbiting around the Lagrangian points, L_4 or L_5.) In phase II, JK found that vortices appeared which periodically on their orbits make close encounters with the planet and cause rapid fluctuating impulses of torque. In phase III the vortices merge into one and impart stronger torque impulses at a slower period. Unfortunately, the results of resolution tests were not conclusive that the physics of the region where the vortices were being generated was well understood. Hui Li and I extended Josef's work to higher resolutions with a more robust and modern code to better understand the region where vortices were emerging. We found that the vortices seen in JK's thesis were generated in regions with important underresolved fine structure, and were not seen in higher resolution simulations. In Section 2, a more detailed description of the disk is given, and in Section 3 potential vorticity is defined and its value to understanding the disk dynamics is explained. In Section 4 the results from our extension of JK's work is presented and in Section 5 unresolved issues and future work is discussed. Section 6 restates the conclusions of our study.

2 Disk Dynamics and Features

In Fig. 2 the disk density is shown to give a more physical picture of the disk and the protoplanet. Following the conventions of JK's thesis, the disk can be divided into

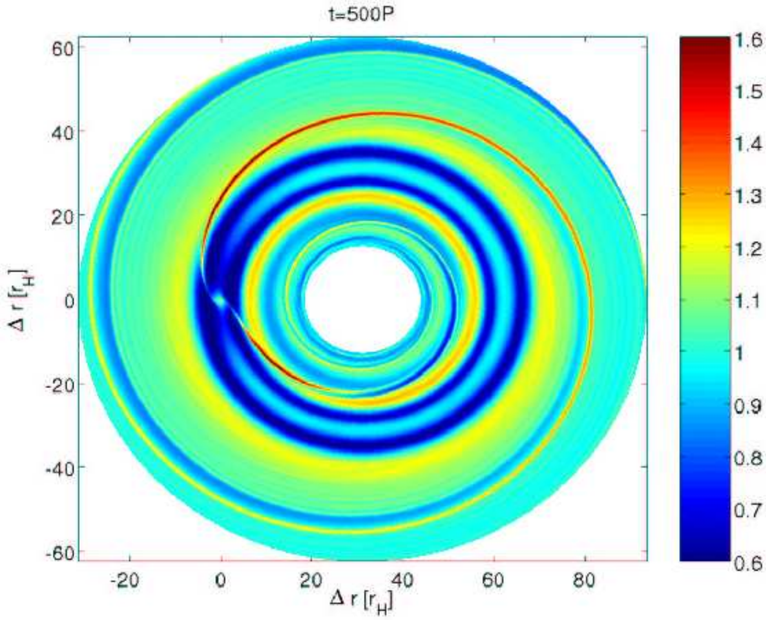

Figure 2: The disk density is shown with a more physically intuitive visualization than representations like Fig. 1. (Figure courtesy of Josef Koller)

three regions: the streaming region $|\Delta r| > \sqrt{12} r_H$ (where r_H is the Roche lobe radius, which is the point where tidal forces are strong enough to rip apart a satellite with no cohesion), the separatix region $r_H < |\Delta r| < \sqrt{12} r_H$ and the horseshoe region $|\Delta r| < r_H$.

The motivation for dividing the disk in this way is also apparent in the potential vorticity (PV) which is the curl of the velocity field (always in the z direction in 2-D) divided by the density. Potential vorticity is presented in Fig. 3 (as well as in Fig. 1 to show the presence of vortices in JK's study). The PV shows important features such as the gas streaming close by the planet at $\phi = \pi$. Another important feature is the spiral shock waves caused by the planet's motion through the disk.

Initially the disk is given a Keplerian angular velocity profile, with the radial velocity component of the gas set to zero. The density is set so that the PV is approximately constant over the disk. The planet's gravitational potential, which is smoothed to prevent a numerical singularity and corrected for 2-D by considering that the disk has a

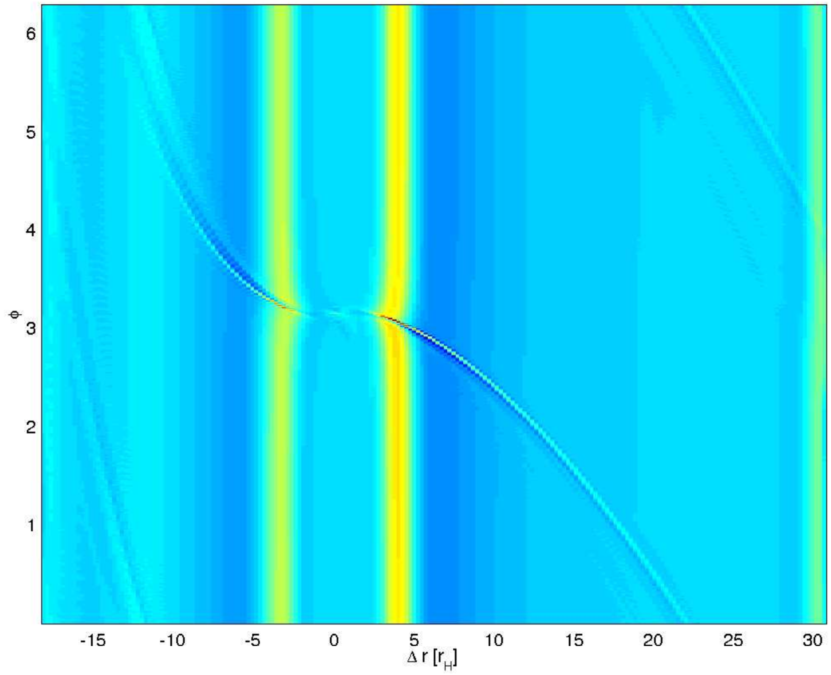

Figure 3: A potential vorticity snapshot of the entire disk. The streaming region is defined as $|\Delta r| > \sqrt{12}r_H$, the separatix region from $r_H < |\Delta r| < \sqrt{12}r_H$ and the horseshoe region from $|\Delta r| < r_H$.

definite scale height. The planet potential is activated over the first few orbits to prevent the disk from being disrupted by a sudden presence of the planet.

The codes used in these simulations solve the equations of hydrodynamics:

$$\frac{\partial \Sigma}{\partial t} + \nabla \cdot (\Sigma \mathbf{v}) = 0 \qquad \text{Continuity Equation (mass conservation)} \qquad (1)$$

$$\frac{\partial \Sigma \mathbf{v}}{\partial t} + \nabla \cdot (\Sigma \mathbf{v}\mathbf{v}) = -\Sigma \nabla \Phi - \nabla P \qquad \text{Momentum Equation} \qquad (2)$$

where Σ is surface density, P is pressure, Φ is the gravitational potential from the star and planet, and $\mathbf{v}$ is the velocity vector. The energy equation is not considered since it is assumed that the disk is isothermal. This is equivalent to assuming that the radiation from the star keeps the disk at a constant temperature and that the heating within the disk is radiated away instantly. It is also important to note that the disk is considered in the inviscid limit. Both the simulations in this study and in Josef's thesis share the same initial conditions, assumptions and geometry; only the codes and resolutions differ.

3 Potential Vorticity (PV)

Potential Vorticity is considered an important diagnostic for investigations of disk dynamics because in an inviscid disk it should be conserved in areas without shocks. This result is derived by first taking the curl of the momentum equation (Eq. (2)). It is perhaps useful to first restate the momentum equation,

$$\frac{\partial \mathbf{v}}{\partial t} + (\mathbf{v} \cdot \nabla)\mathbf{v} = -\frac{1}{\Sigma}\nabla P - \nabla \Phi \tag{3}$$

and taking the curl becomes,

$$\frac{\partial \omega}{\partial t} - \nabla \times (\mathbf{v} \times \omega) = \frac{\nabla \Sigma \times \nabla P}{\Sigma^2} \tag{4}$$

where the vorticity is defined $\omega = \nabla \times \mathbf{v}$ and the gravitational term has dropped out since $\nabla \times (\nabla \Phi) = 0$. The source term on the right hand side of Eq. (4) is normally zero except in a shock where pressure and density gradients will be misaligned. When this source term is zero the gas is referred to as having a barotropic equation of state. It is also worth noting that the mathematics and concepts behind Eq. (4) are applicable to flux freezing in magnetohydrodynamics, and the Biermann Battery (discussed in Orban 2004).

In barotropic conditions the vorticity equation can be manipulated to become,

$$\frac{\partial \omega}{\partial t} + (\mathbf{v} \cdot \nabla)\omega - (\omega \cdot \nabla)\mathbf{v} + \omega(\nabla \cdot \mathbf{v}) = 0 \tag{5}$$

while the continuity equation (Eq. 1) can be rewritten as

$$\frac{\partial \Sigma}{\partial t} + \Sigma \cdot (\nabla \cdot \mathbf{v}) + \mathbf{v} \cdot \nabla \Sigma = 0. \tag{6}$$

Except near shocks or compression $\nabla \cdot \mathbf{v}$, is usually zero. (The minimum of $\nabla \cdot \mathbf{v}$ at each radius was actually used to find the site of the shock in the next section. Physically this is the site of maximum compression. The assumption that $\nabla \cdot \mathbf{v} = 0$ is equivalent to assuming that the gas is incompressible.) Substituting $\nabla \cdot \mathbf{v} = 0$ into Eqs (5) and (6), and acknowledging that in 2-D the vorticity only has a z component, can be used to simplify those equations:

$$\frac{\partial \omega}{\partial t} + (\mathbf{v} \cdot \nabla)\omega = 0 \tag{7}$$

$$\frac{\partial \Sigma}{\partial t} + \mathbf{v} \cdot \nabla \Sigma = 0 \tag{8}$$

using $(\mathbf{w} \cdot \nabla)\mathbf{v} = 0$ from the 2-D restriction. The vorticity, ω, can now essentially be treated as a scalar, and by dividing Eq. (7) by Σ, and multiplying Eq. (8) by ω/Σ^2, setting them equal to each other (they are both equal to zero after all) and doing some manipulation the following equation can be obtained,

$$\frac{\partial}{\partial t}(\frac{\omega}{\Sigma}) + \nabla \cdot (\frac{\omega}{\Sigma}\mathbf{v}) = 0 \tag{9}$$

which bears striking resemblance to the continuity equation. Essentially, the quantity ω/Σ is conserved a similar way that mass is conserved if there are no shocks around. In Josef Koller's thesis a more detailed derivation is given that even lifts the $\nabla \cdot \mathbf{v} = 0$ restriction, but has the same qualitative conclusion.

With this knowledge it is useful to glance back at Figs. 1 and 3 and note that if vortices are present they will have constant constant PV except in periodic passes through the shock. Also notice that most of the PV is generated in the spiral shock waves. An azimuthal average of the PV across the disk as shown in Fig. 4 is also useful. It confirms that the spiral shocks deposit potential vorticity in the streaming regions, but also shows that the vortices emerge from regions where the azimuthally averaged PV has a valley. Though more quantitative treatment is given in the next section, the most troubling result from JK's thesis was the lack of convergence of these valleys. High resolution simulations presented in the next section have shown that the

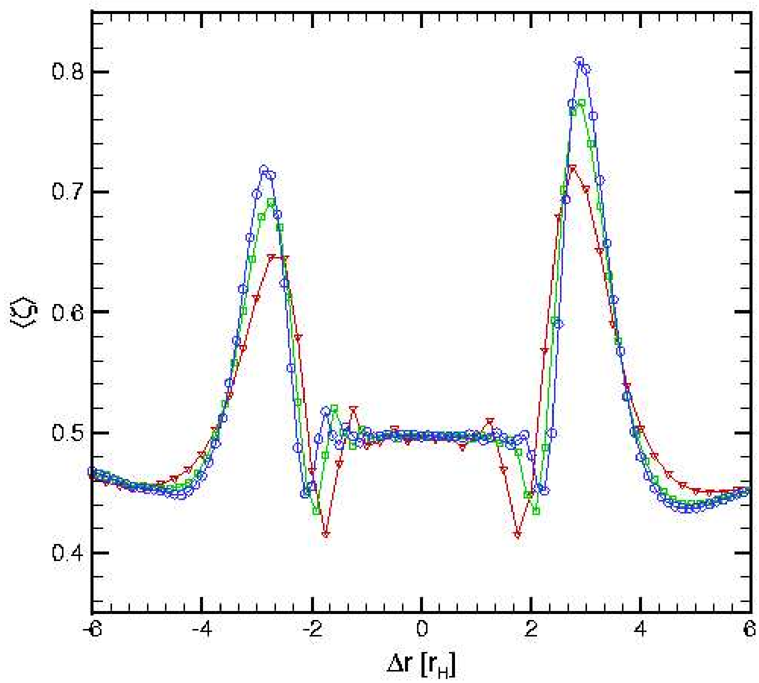

Figure 4: Azimuthally averaged potential vorticity for 200x800, 300x1200, and 400x1600 resolutions from Josef Koller's thesis work. The vortices seen in Fig. 1 originate in the valleys near $\Delta r = \pm 2 r_H$. The lack of convergence of the valleys is concerning for understanding the physics of this region. (Figure courtesy of Josef Koller)

valley disappears, and has also brought to light the reasons for this effect, which is due to the convergence of some of the finer structure of the shock.

It is important to mention here that vorticity and potential vorticity are difficult quantities. Vorticity itself is calculated from derivatives of the velocity field which creates error through the nature of finite differencing and by dividing vorticity with a density field as shown in Fig. 5. Even two smooth vorticity and density distributions can create what appear to be oscillations in PV. We do not find that these sorts of issues to detract from the results presented here, or cast doubt on the accuracy of the codes, but it is frustrating that quantities as valuable as vorticity and PV suffer from these numerical effects.

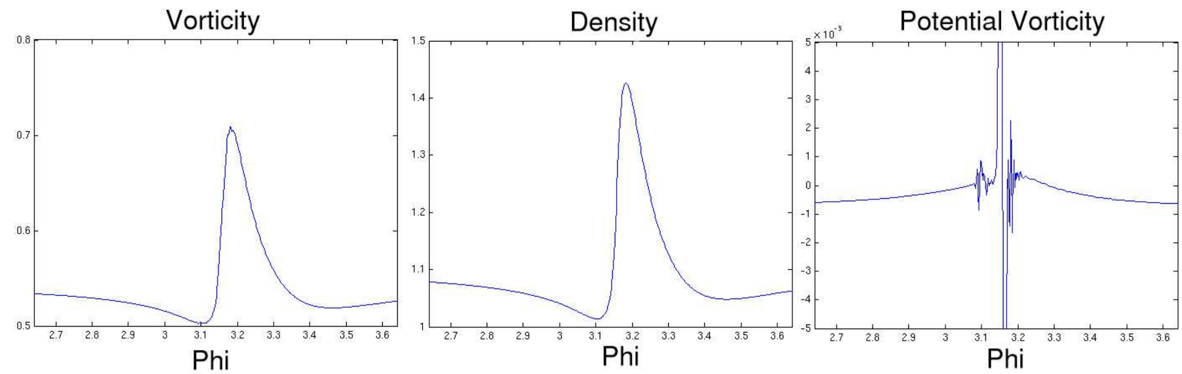

Figure 5: The vorticity, density and potential vorticity profiles through a shock at constant radius ($\Delta r = -2.5 r_H$) is shown. The smooth vorticity and density profiles do not create a smooth potential vorticity profile.

4 Primary Results

The high resolution simulations present two main puzzles: in the azimuthally averaged PV plot (shown in Fig. 6) the valleys completely disappear, and in Fig. 7, a snapshot of PV at the same time, a distinct "finger" of PV extends from the spiral shock wave at $\Delta r = \pm 3 r_H$ into the separatix region. This feature does not appear in Figs 1 and 4 which are from JK's thesis work.

A few important questions can be asked about this feature: Is it a shock? If so, how strong is it and where does it start? And since PV is conserved why doesn't the finger heavily pollute the separatix region with PV?

To answer any of these questions a reliable way to locate the shock position and finger must be found. In JK's thesis the maximum density at each radius was used to do this, but at higher resolutions the minimum of $\nabla \cdot \mathbf{v}$, in other words the maximum compression, was found to locate the shock and finger more accurately than the maximum density. Figure 9 contrasts the shock positions as determined by these methods. It is apparent that $\nabla \cdot \mathbf{v}$ is a better indicator for $|\Delta r| < 3 r_H$. The max density method is strongly affected by the overdensity of material held in the planet's gravitational potential.

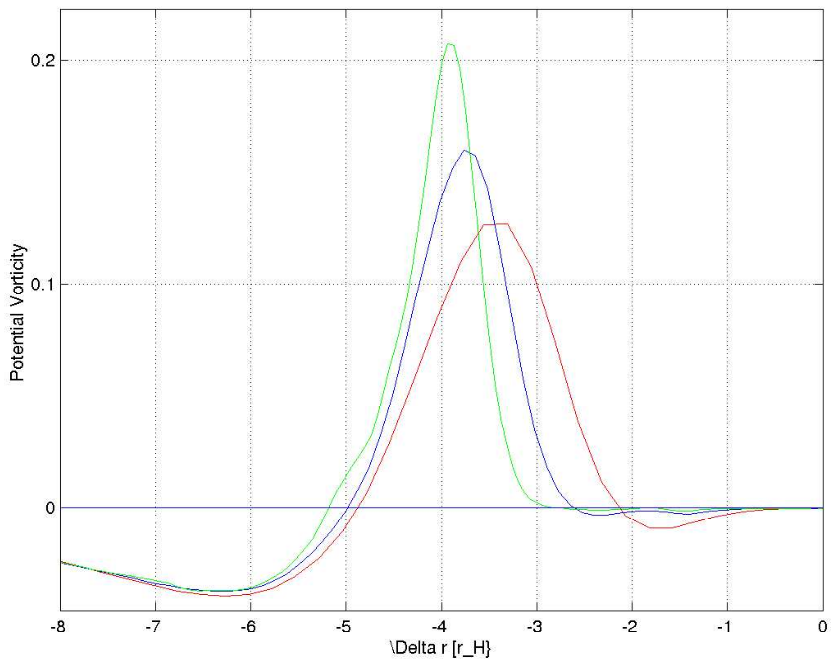

Figure 6: The azimuthally averaged potential vorticity for 200x800 (red), 400x160 (blue), and 800x3200 (green) resolutions is shown for one side of the planet after 100 orbits.

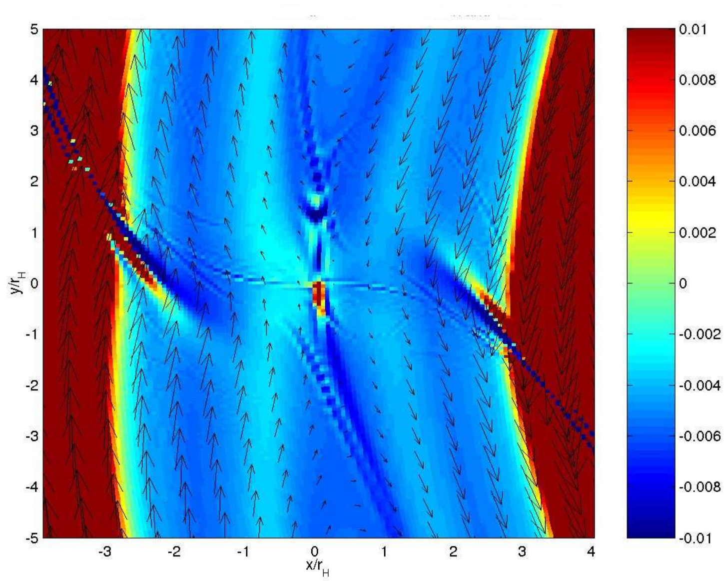

Figure 7: A potential vorticity snapshot of the disk including velocity vectors for the 800x3200 run after 100 orbits.

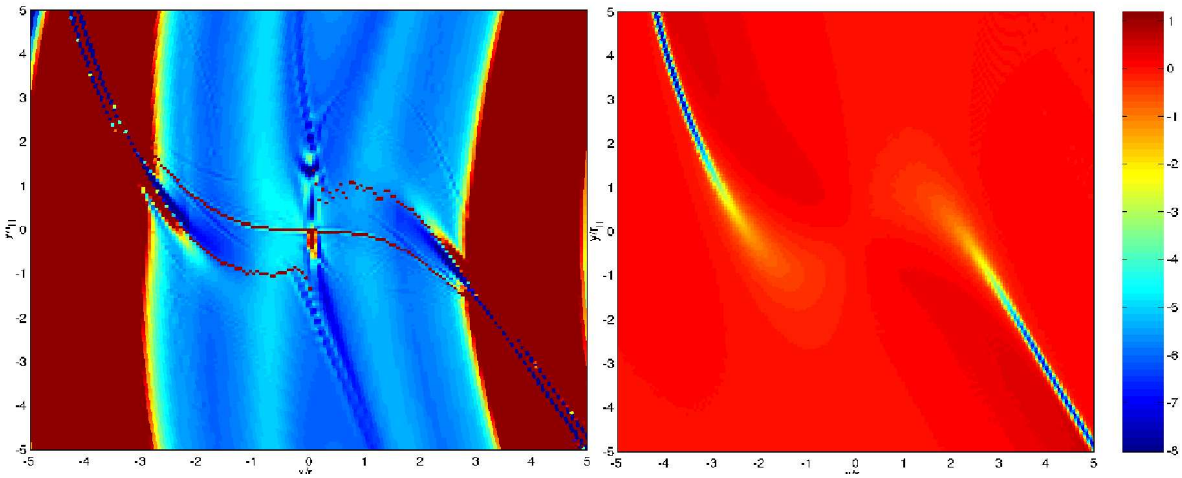

Figure 8: One the left the shock positions determined by $\nabla \cdot \mathbf{v}$ and maximum density near the planet are indicated with potential vorticity in the background. The shock position determined by the max density goes through the center of the planet, while the $\nabla \cdot \mathbf{v}$ tracks the finger rather well. The right side shows a snapshot of $\nabla \cdot \mathbf{v}$ in the same region.

With the spiral shock wave and finger position determined, the relative speed of the incident gas on this boundary can be determined. If this relative speed exceeds the sound speed, which is constant across the disk, then a shock is present. A plot of the perpendicular Mach number, $M_\perp$, verses radius is shown in Fig. 9. From this plot it is learned that $M_\perp$ stays below 1.5 so it is not an extremely strong shock, and that the shock starts possibly as close as $-1.5r_H$. The scatter of $\nabla \cdot \mathbf{v}$ in Fig. 8 casts doubt on the precise distance where the shock starts, but it is still apparent that the fingers of PV are in shocked regions.

This result makes the question of why the finger does not pollute the separatix region more perplexing since a shock is present so PV is being generated there. A plot of the streamlines is very illuminating to this issue. Figure 10 shows the streamlines near the planet. The planet's gravity attracts the gas and deflects it closer to the planet, but it returns to essentially the same orbit after the encounter. Streamlines that are deflected

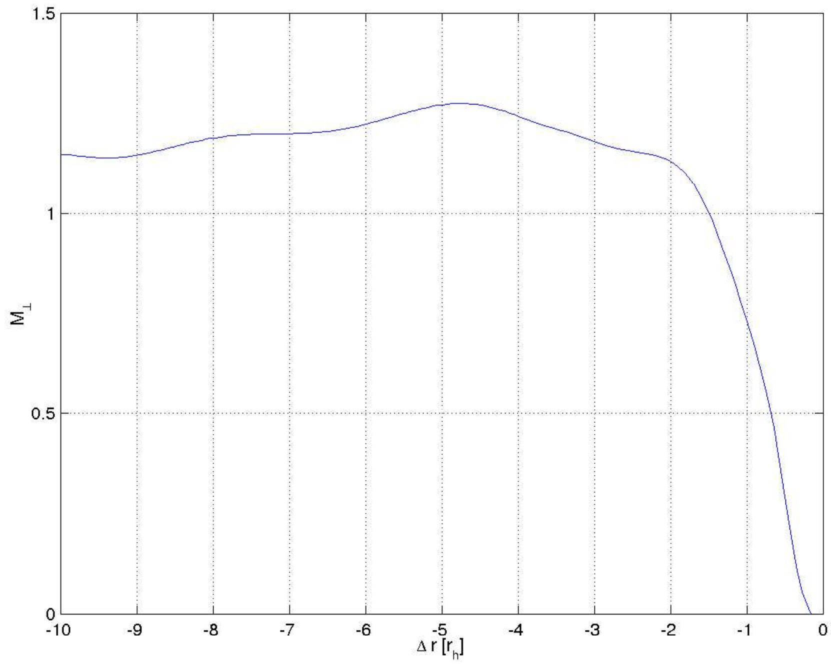

Figure 9: The perpendicular Mach number for the incident gas on the shock boundary determined with $\nabla \cdot \mathbf{v}$. The gas becomes supersonic near $-1.5r_H$, so the finger is definitely in a shocked area.

through the finger clearly return to the streaming region where the high PV is seen. Potential vorticity is not deposited in the separatix region.

The vorticity jump across a shock can be calculated with a very useful result from Kevlahan (1997),

$$\Delta\omega = -\frac{\delta^2}{1+\delta}\frac{\partial v_\perp}{\partial \tau} \tag{10}$$

where $\delta = \Sigma_2/\Sigma_1 - 1$, and Σ_2 corresponds to the density in the post shock region, while Σ_1 corresponds to the pre-shock region. The $\partial v_\perp/\partial\tau$ term the derivative of the perpendicular component of the wind tangential to the shock. Since $\Sigma_2/\Sigma_1 = M_\perp^2$, Eq. (10) can be rewritten,

$$\Delta\omega = -\frac{(M_\perp^2 - 1)^2}{M_\perp^2}\frac{\partial v_\perp}{\partial \tau} \tag{11}$$

This equation can be used to better understand the azimuthally averaged PV plot in Fig. 7. The flat profile for $\Delta r > -2r_H$ can be explained since even if the shock starts

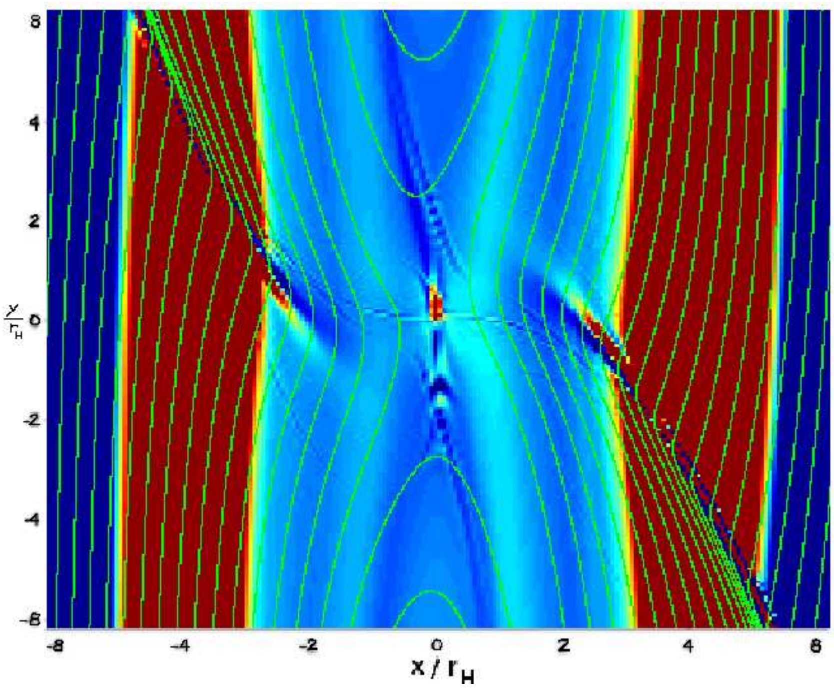

Figure 10: Streamlines are shown in green over the PV for an 800x3200 run. The streamlines show that the gravitational potential of the planet bends the path of the gas streaming past the planet, but after the encounter the gas returns to roughly its original radius. This explains why the finger does not severely pollute the separatix region with PV.

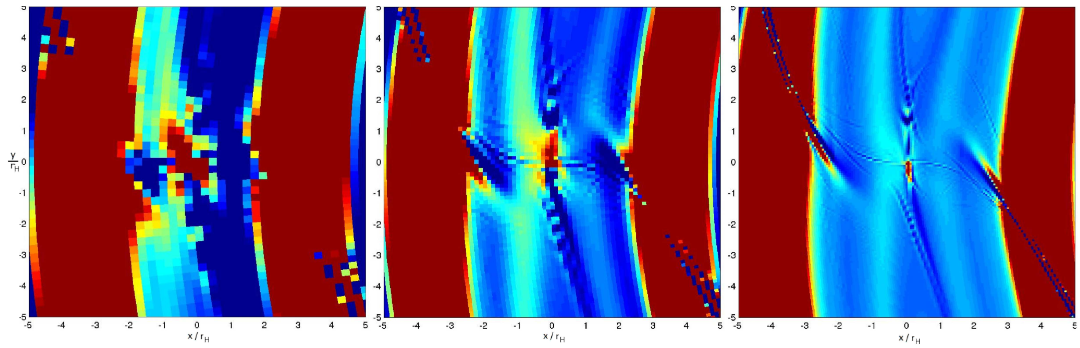

Figure 11: Potential vorticity snapshots of the planet region for 200x800, 400x1600, and 800x3200 resolutions after 100 orbits. Notice that the large blue negative PV regions near the planet in 200x800 grow smaller with increasing resolution. This effect is the key to explaining the lack of convergence of the azimuthal average PV from simulations in Josef Koller's thesis work such as Fig. 4.

as close as $-1.5r_H$ the streamlines will carry PV further away, and closer in to the planet there is no shock, so there should not be a vorticity jump. The $\partial v_\perp/\partial\tau$ term is proportional to the vorticity jump and can be determined from the plot of $M_\perp$ verses Δr in Fig. 9 and compared to Fig. 6. The peak in Fig. 9 at $\Delta r = -5r_H$ lines up with the zero crossing in Fig. 6, and a large negative slope around $-4r_H$ matches up with the peak in Fig. 6. These points seem to be well understood in the azimuthally averaged PV. This correspondence was also noticed in JK's thesis.

Comparing Fig. 6 to Fig. 4 taken from JK's thesis, the 200x800 and 400x1600 runs in Fig. 6 show similar features as those in JK's simulations, but in the 800x3200 run the valley has disappeared. The finger is present near the same position where valleys appear in the lower resolution runs. Snapshots of the PV near the planet are presented for different resolutions in Fig. 12. As the resolution increases, the structure becomes more defined, but it is also apparent that the "blue area" behind the finger grows smaller with increased resolution, and is quite large in the 200x800 run. This effect is responsible for the convergence in Figs. 4, and 6. Since the blue area is large in the 200x800 resolution shown in Fig. 11, this creates a corresponding dip in the azimuthally averaged PV. In 400x1600 the blue has shrunk, but is still significant enough to cause a noticeable dip, and in 800x3200 it has nearly disappeared. This result is also seen by averaging the PV only over the azimuth in the vicinity of the planet. Essentially the same profile is seen, but is shifted closer to the planet because of gravity. There are no other sources of PV in the separatix region, so the profile is largely the same shape through the rest of the disk.

The disappearance of the valley at high resolutions implies that the vortices seen in JK's simulations were generated in areas suffering from now understood numerical effects. This has important ramifications for the torque on the protoplanet which is thought to be primarily caused by interactions with these vortices. It remains to be seen if the high resolution simulations presented here carried out to longer times would eventually create similar behavior in the torque evolution since it is expected that vortices will be generated from the other peaks and valleys of the azimuthally averaged PV, but after a longer time.

5 Unresolved Issues and Further Work

With the capabilities of the codes used in this research combined with the insight gained from analytic expressions such as Eqs. (9) and (11), many other explorations of disk physics with embedded protoplanets can be accomplished. In JK's thesis, multiplanet simulations were investigated as well as the effect of varying a variety of disk constants such as sound speed, and the mass ratio of the planet to the star (which was always taken to be 10^{-4} in this study).

Josef mentioned that lifting the requirement that the planet be fixed at a certain radius allowing it to actually migrate may find more complicated interactions between the planet and the disk. The torque evolution could be also investigated at higher resolutions as mentioned in the previous section.

In this study the sound speed was set to 0.065 which is large enough to prevent the spiral shock wave from originating near the planet so that the focus remains on understanding the shock wave itself rather than the interactions between the shock wave and the planet's roche lobe region. A wider range of sound speeds were considered in JK's thesis. There is no lack of interesting ideas for future studies.

Despite this optimism there are still some unresolved numerical issues. The most concerning is the growth rate of the Azimuthally averaged PV. Figure 12 plots the PV growth of the peak of the azimuthally averaged PV plot as time evolves. The slope continues to rise for higher resolutions instead of converging. This problem was already apparent in Figs. 4 and 6.

The simulations presented here use a total variational diminishing code (TVD) developed by Shengtai Li at Los Alamos National Laboratory. The simulations in JK's thesis used a highly optimized hybrid Lax-Wendroff/Lax-Friedrich code. A classic test of hydrodynamics codes is its ability to capture shocks. The two can be compared by viewing the vorticity profile at constant radius across a shock in the protoplanet setup. This is shown in Fig. 13 for the TVD code and a pure Lax-Wendroff code. It is obvious that TVD does a much better job at capturing the shock.

Another concerning numerical issue is PV generation from the planet itself. The planet's presence is only communicated to the disk by its gravitational potential which should not introduce PV since $\nabla\times(\nabla\Phi) = 0$, but in Fig. 14, an early PV snapshot (after 20 orbits), it is obvious that PV is being generated there. The azimuthally averaged PV

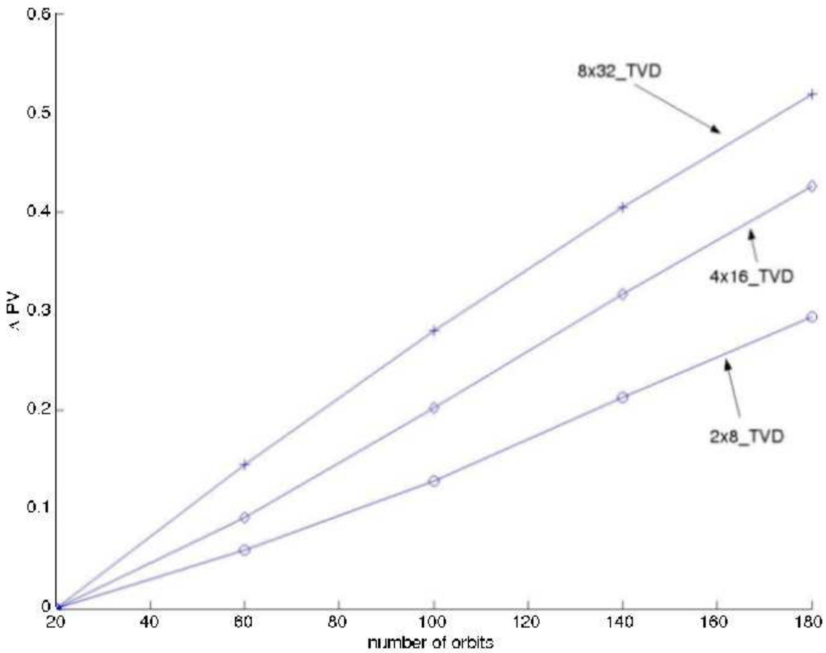

Figure 12: The growth rate of the peak of the azimuthally averaged potential vorticity. The y-axis unit is the difference in potential vorticity from the value at 20 orbits. Circles mark the measurements from the 200x800 simulations, diamonds for 400x1600, and pluses for 800x3200.

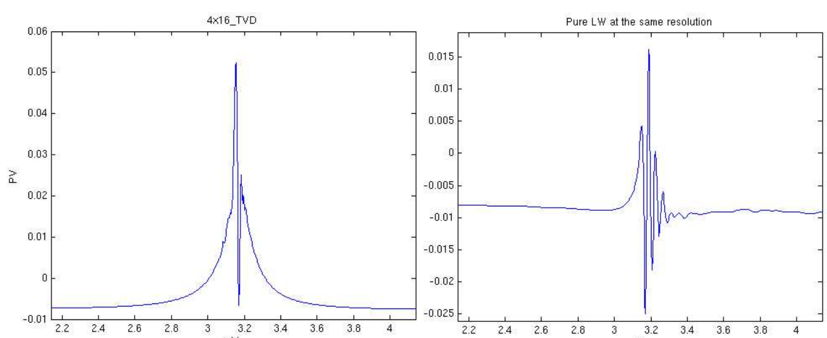

Figure 13: The vorticity profile across a shock in the protoplanet setup at constant radius. The left plot shows the output from the TVD code, and the right plot shows output from a pure Lax-Wendroff method. The Lax-Wendroff method suffers from severe oscillations.

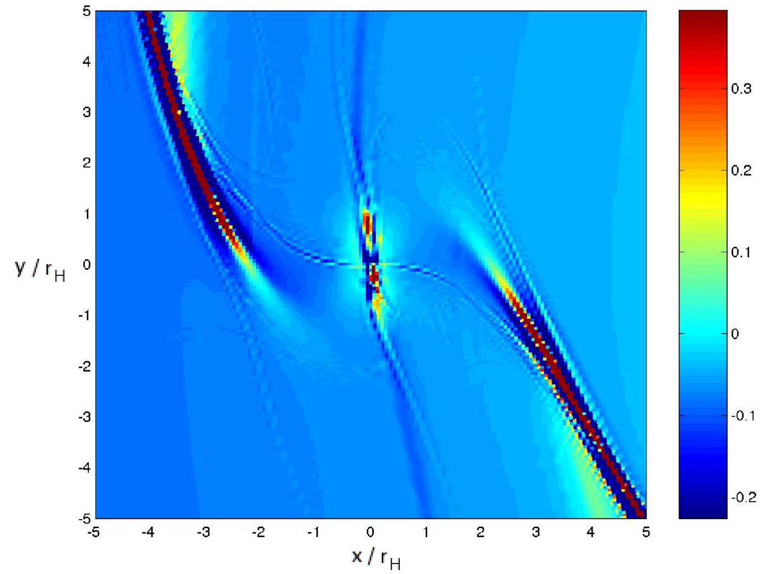

Figure 14: The potential vorticity from the 800x3200 run after 20 orbits is shown. High potential vorticity is seen near the planet, and streaming away from it, indicating that potential vorticity is being generated there- a purely numerical effect.

does appear to be very sensitive to this effect, but nonetheless special treatments of the gravitational potential may be able to prevent it.

6 Conclusions

Further investigations of disk dynamics with an embedded protoplanet have been conducted to address convergence issues in the simulations in Josef Koller's PhD. thesis. More modern and robust codes were used at high resolutions to show that the lack of convergence is due to unresolved structures in the co-orbital region. At the highest resolution the "valley" in the azimuthally averaged potential vorticity where vortices previously emerged has disappeared. This discovery has important consequences for the torque evolution of the protoplanet since close interactions with vortices would cause large impulses of torque. Some numerical issues still exist such as the convergence of the growth rate of potential vorticity and generation of potential vorticity at the planet, but the mystery of the convergence issues in Josef Koller's PhD. thesis has been solved.

Much thanks goes to my adviser, Hui Li, for his mentoring and patience and to the T-6 group at Los Alamos National Laboratory for supporting me.

7 Appendix A

All of the analysis presented in this report was done in MATLAB. A number of scripts have been developed and are accessible as world readable from the home directory of corban in T-6 and T-7. Until December 2004 the scripts are also posted to the web at `netfiles.uiuc.edu/corban/www/Orban_scripts.tar`. They are designed to create plots from the ASCII data output of the protoplanet simulations and are fairly well commented. Scripts rather than functions are used so that the matrices that are loaded globally and can be accessed by the user after the script is run.

Script Name	Description
planet2.m	The swiss army knife of scripts. Can create 21 different plots from the data. Ex: Fig. 2, 6, 7, 14. Consider planet2_lean.m for large data sets.
growth_res.m	Used in conjunction with growth.m to create plots of the growth rate of the potential vorticity. Ex: Fig. 12.
snapshots_PV.m	Used to create a collage of snapshots of the potential vorticity at different resolutions and times. The HTML file, collage.html, is a convenient display of the output of this plot (which are jpeg images). Ex: Fig. 12
vorticity_quant_2x8.m, vorticity_quant_4x16.m, vorticity_quant_8x32.m	These scripts create $M_\perp$ vs r plots for different resolutions, such as Fig. 9. There is not a general code for the three resolutions since the polynomial fit often needs to be checked by the user. An uncertain shock position close to the planet can lead to strange results. Use snapshots_Merp.m with collage_Mperp.html to make this plot for a variety of resolutions and times automatically.

8 References

The Extrasolar Planets Encyclopedia (http://www.obspm.fr/encycl/encycl.html)

Hollenbach, D.J., Yorke, H.W., & Johnstone, D. 2000, Protostars and Planets IV, 401

Kevlahan, N. K.-R. 1997, J. Fluid Mech., 341, 371

Koller, J. 2004, PhD. thesis, Rice University.

Orban, C.M. 2004, "Modelling Protogalactic Collapse and Magnetic Field Evolution with FLASH.", Preliminary summer research report, University of Illinois Urbana-Champaign.

Udry, S., Mayor, M., & Santos, N.C. 2003, A&A,407,369